

# Crystallization behavior, thermal property and enzymatic degradation of PVP/amylose in the presence of graphene oxide nanosheets



Mohammad Taghi Taghizadeh<sup>\*</sup>, Reza Abdollahi

Department of Physical Chemistry, Faculty of Chemistry, University of Tabriz, Tabriz, Iran

## ARTICLE INFO

### Article history:

Received 17 January 2015

Received in revised form

7 March 2015

Accepted 20 March 2015

Available online 28 March 2015

### Keywords:

Amylose

GO nanosheets

Nanocomposite

PVP/amylose

Crystallinity

## ABSTRACT

The PVP/amylose composite films with different amounts of graphene oxide (GO) were prepared by means of a solution casting method. The solution of PVP/amylose/GO was exposed to ultrasonic irradiation (10, 30, 50, and 70 W) and then prepared for casting. The crystallization behavior, thermal stability and enzymatic degradation of PVP/amylose were investigated with differential scanning calorimetry (DSC), X-Ray diffraction (XRD), scanning electron microscopy (SEM), and FTIR spectroscopy. XRD patterns monitored that the addition of GO induced a layered structure to the PVP/amylose composite films. This result indicated that GO nanosheets were uniformly dispersed into the composite network. The thermal properties measured by DSC showed that the glass transition temperature ( $T_g$ ) was shifted to a lower temperature with the humidity percent increasing. DSC thermograms for PVP/amylose/GO showed an endothermic reaction and reduction in peak temperature, revealing that GO increased the thermal stability of PVP/amylose composite films. FTIR analysis suggests that PVP/amylose composites become more resilient to enzymatic attacks as the content of GO reaches higher, being related to the reduction of Amylose–Amylose interactions in the presence of GO nanosheets. These results indicate that this approach is an efficient method to improve the properties of PVP/amylose.

© 2015 Elsevier Ltd. All rights reserved.

## 1. Introduction

Amylose is the linear component of common starch and characterized by its straight chains which are made up of  $\alpha$ -(1  $\rightarrow$  4) bond glucose molecules and it has drawn much attention due to its unique qualities, such as its film-forming ability and strength [1]. Pure amylose films, with good tensile strength and low water vapor and oxygen permeability can be applied to seal materials, packaging materials, and biomaterials. The mechanical properties of starch based materials have been investigated by a number of researchers and there have been studies on the crystallinity of high amylose films [2,3]. In amylose solution, gelatin occurs by a short-time scale phase separation in polymer-rich and polymer-deficient regions by longer time scale crystallization in the polymer-rich phase [4].

Thus, a big challenge in the supplying process of amylose/GO nanocomposite is the dispersion of the GO nanoparticles into the matrix material, because of the two phase behavior of amylose

solution. On the other hand, well separated nanoparticles can lead to unique and new properties of the composite [5,6]. At present, a number of methods are used for the dispersion of particle agglomerates in a liquid, in which ball mill and ultrasonic are the most common methods. Ultrasonic irradiation helps to make a homogeneous network and reduce the phase separation of amylose solution that results in a coalescent forming of the films [7,8]. Another role of sonication is the help to the dispersion of nanoparticles agglomerates in the matrix. The applying of acoustic waves to the polymer-nanoparticle emulsion, caused to the unstable cavitation bubbles, growing in the ultrasonic field [9]. The cycle of growing and collapsing of these bubbles causes locally extreme condition as a very high local pressure and temperature, called hot spot [10]. These hot spots are responsible for the dispersion of the particles in the liquid. The shock waves from the implosive bubble collapse in combination with micro-streaming generated by cavitation oscillations lead to dispersion effects [11]. Yasmin et al. reported dispersing expanded graphite in epoxy resin by sonication method [12]. They found that an improvement in elastic properties of nanocomposites occurred when the nanoparticles were dispersed by ultrasonic treatment. This could be attributed to a good dispersion of nanoparticles and good interfacial adhesion between

<sup>\*</sup> Corresponding author. Tel.: +98 41133393137; fax: +98 41133340191.

E-mail address: [mtaghizadeh@tabrizu.ac.ir](mailto:mtaghizadeh@tabrizu.ac.ir) (M.T. Taghizadeh).

the particles and epoxy matrix so that the mobility of polymer chains is restricted under loading [13].

Graphene, a kind of two-dimensional nanofiller with a thickness of one atomic layer, is a single layer of  $sp^2$ -hybridized carbon atoms. In recent years, much attention and interest have been given to graphene because of its excellent mechanical, electronic and thermal properties [14–17]. The ability of graphene to enhance the properties of polymer composites has also been reported [18]. There are several ways to prepare graphene, including the use of graphene oxide (GO) [19–22]. Since graphene oxide (GO) can be synthesized on a large-scale, it is commonly used to prepare reduced GO. GO can be uniformly dispersed in water and some organic solvents, because its sheets contain various oxygen functional groups, such as hydroxyls, epoxides, carbonyls and carboxyls. These groups change the van der Waals interactions between the layers of graphene and improve the solubility of GO [23]. The existence of oxygen functional groups also helps GO bond to some natural polymer matrices which have led to the fabrication of graphene-based materials by solution casting; applications of these graphene oxide biocomposites have been discussed [24–26]. GO nanosheets added into polymer matrices can increase the tensile strength and thermal stability of the matrices [27–29].

Despite of good tensile strength and high crystallinity of pure amylose, aggravation of GO into an amylose matrix improved the mechanical properties of the amylose/GO composite films this could be related to electrostatic and hydrogen bonding interactions between the hydroxyl groups of the amylose and oxygen functional groups on the GO nanosheets. Use of ultrasonic wave as a homogenizer to supply a uniform state of well-dispersed network has never been reported. A simple method of preparing GO/amylose films via casting blends of GO into aqueous amylose solutions pretreated by sonolysis is reported. The prepared films were characterized by X-ray diffraction, Differential scanning calorimetry and FTIR spectroscopy. The influence of ultrasonic power on the properties of PVP/amylose/GO nanocomposites was investigated. Also, the amount of GO loading on the, enzymatic degradation and moisture uptake of the PVP/amylose/GO films were studied.

## 2. Experimental

### 2.1. Materials

Amylose ( $C_6H_{10}O_5$ )<sub>n</sub> purified from potato starch, with a purity of 99% was purchased from Gamay Industrial Technology Co. Ltd, Shanghai-China. The purchased amylose sample was dissolved in dry DMSO at the concentration of 1 mg/mL and centrifuged at 2000 × g for 3 min to remove any insoluble impurities. Subsequently, Ethanol was added to the supernatant to precipitate the amylose, which was dried under high chromatography (SEC), using monodisperse PEG ( $M_w = 20,000$  Da) as a calibration standard and water as a mobile phase. SEC results revealed that the amylose has an average molecular weight ( $M_w = 48,600$  Da) and polydispersity of 3.78. Graphite was purchased from Aldrich. Other chemicals were supplied from Merck. All chemicals were of analytical grade and used as received. Doubly distilled water was prepared using a laboratory distiller device.

### 2.2. Methods

#### 2.2.1. Preparation of the amylose solutions

0.5 g of amylose was dispersed in 100 mL distilled water, degassed and heated to 100 °C before stirring magnetically. The mixture was stirred and heated at  $90 \pm 5$  °C for 8 h to yield a transparent solution and the cooled to the room temperature prior to use.

#### 2.2.2. Preparation of GO nanosheets

The process of GO preparation was developed by researchers based on the Hummers method [30,31]. In brief, 1 g of pure graphite was added to a flask containing 25 ml concentrated  $H_2SO_4$  at 0 °C (ice bath), followed by the addition of  $NaNO_3$  (0.5 g). Then, 3 g  $KMnO_4$  was added gradually with stirring at a fixed temperature of solution below 20 °C controlled by a thermometer for 2 h. Then, the temperature increased to 35 °C and the solution was stirred for 30 min and excess distilled water was added to the mixture and the temperature was then increased to 90 °C and stirred for 1 h. Finally, 30%  $H_2O_2$  was added until the color of the mixture changed to brilliant yellow and there was no gas being produced. The product was passed from the filter and then washed with HCl solution to remove the metal ions and then washed distilled water to remove any acid remained. The resulting filter cake was dried and again dispersed into water. The final product was sonicated for 3 h by an ultrasonic transducer (Dr. Hielscher Ultrasonic Processor UP200 H; frequency of 24 kHz) at 20 °C at 60 W and a suspension of GO sheets was obtained.

#### 2.2.3. Preparation of the GO/amylose films

GO/amylose films with different amount of GO loadings (0.0, 0.2, 0.4, 0.6 and 0.8 wt %) was prepared. Within the preparing of GO/amylose films ultrasonic treatment carried out as follows: at first step the 2 g amylose was dispersed into 200 mL distilled water and 20wt% PVP was added into the solution and desired amount of GO was subsequently added to the amylose suspension. Then, the obtained suspensions were exposed at ultrasonic radiation in 10, 30, 50 and 70 W power of sonication at the aqueous media for 30 h and stirred and simultaneously, fixed temperature by means of a thermostat at 30 °C. The homogenous solution was poured on a PVC plate and dried at room temperature for 4 days to form a film. The thickness of prepared PVP/amylose/GO films was approximately 50  $\mu$ m.

#### 2.2.4. Fourier transform infrared (FTIR) spectroscopy

The FTIR spectra of PVP/amylose/GO films after regular intervals of exposure in  $\alpha$ -amylase were recorded by Shimadzu RF50 FTIR spectrophotometer using KBr pellets. The scanning range was 4000–500  $cm^{-1}$ . Samples of PVP/amylose films that were treated with enzyme for 0, 1, 3, 5, 7, 14, 24 and 48 h were prepared for FTIR analysis. Before the analysis, the films were dried under vacuum at 30 °C for 24 h to eliminate traces of moisture.

#### 2.2.5. X-ray diffraction

X-ray diffraction analysis was performed with a Siemens XRD-5000 diffractometer operated at 40 kV, 50 mA at 25 °C with a graphite-filtered  $Cu K_{\alpha} = 1.54$  Å target radiation. The relative intensity was recorded in the scattering range ( $2\theta$ ) of 0–40°.

#### 2.2.6. Differential scanning calorimetry (DSC)

The glass transition temperature of the films was determined by DSC thermograms. The samples were analyzed using Pyris 1 DSC (Perkin Elmer, USA). The system was calibrated for temperature and heat flux with indium (transition point: 156.6 °C, heat of fusion = 3.28  $kJ mol^{-1}$ ). The samples (8–15 mg) were weighed in aluminium pans and hermetically sealed and an empty pan was used as the reference. Scans were carried out over the temperature range of 0–140 °C at a heating rate of 10 °C  $min^{-1}$  under nitrogen atmosphere. During each run the nitrogen flow rate was 24  $cm^3/min$ . The  $T_g$  was determined at the onset of the endothermic shift in heat flow and the end of the transition were determined and the area under the curve was used as  $\Delta H$ .

### 2.2.7. Moisture content determination

The moisture contents of both the PVP/amylose films alone and in the presence of GO nanosheets were determined by gravimetric method. The measurements were performed in different environments that contained a saturated salt solution to give the desired relative humidity (RH) (MgCl<sub>2</sub>: RH = 33%; NaBr: RH = 53%; KBr: RH = 81%). The initial weight of the dry films was determined after being dried to a constant weight in a vacuum oven at 60 °C for 24 h. The weighed samples were then placed in incubators at 25 °C at different relative saturation humidity and they were weighed, at some intervals until their weights became constant. Tests were conducted in triplicates and average values are reported. The value of moisture absorbability (Ma) was calculated as follows:

$$Ma\% = \left[ \frac{W - W_0}{W_0} \right] \times 100$$

### 2.2.8. Scanning electron microscopy (SEM)

The morphology of the surface of the films was investigated using a scanning electron microscope. The sample was coated with pure Ag using a sputter coater (SCD500 sputter coater, Bal-Tec, Switzerland). The laying down of Ag was carried out using the evaporation of the metal under a high vacuum, to give a thickness of around 100 Å. The samples were observed and photographed in an environmental SEM (PhilipsXL-30) with an accelerating voltage of 30 kV and working distance of 10 mm.

## 3. Results and discussion

### 3.1. Thermal properties of the PVP/amylose/GO films

The advantage of adding GO into PVP/amylose composite is the improving of compatibility via an electrostatic interaction between the abundant hydroxyl groups of amylose and oxygen functional groups located on the GO nanosheets. Furthermore, the establishment of hydrogen bonds could be improved the properties of these composite films [32]. The presence of PVP in the composite matrix, supplied an excellent film-forming ability and adhesive behavior for the PVP/amylose/GO nanocomposite films. This may be related to the conductive properties and the amorphous structure of PVP that candidate it as an ideal polymer for contributing in composite materials applications [33,34].

The first heating thermograms obtained during the melting of PVP/amylose films with different moisture content are presented in Fig. 1. In moisture content range between 33% and 81% a clear single endothermic relaxation peak is observed in each sample. As the moisture content of the samples increased, thermograms peak decreased from 85.5 to 54.3 °C. This variation shows the relation between T<sub>g</sub> values of PVP/amylose composites and water content. Thiewes et al. demonstrated that a carbohydrate–water interaction is the main source of this correlation and the increase of moisture content shifted the enthalpy relaxation to a bimodal endothermic transition at lower temperatures [35]. Recently, a two-phase enthalpic relaxation for the transformed cassava starch (TCS) containing 10.6% moisture was reported by Perez et al. [36]. They discovered that the higher transition temperature is more dependent on moisture content than the lower temperature one.

The corresponding thermograms of the PVP/amylose/GO contained different amount of GO (0.2, 0.4, 0.6 and 0.8wt%) are also shown in Fig. 2. As it has been shown, DSC thermograms of PVP/amylose film and also films that consist of different amounts of GO exhibited endothermic transition peaks. As usual, the low temperature endothermic peak is attributed to the melting of the

crystalline lamella, while the high temperature peak ascribed to the dissociation of the PVP/amylose composite or PVP/amylose/GO nanocomposites. The melting temperature (T<sub>m</sub>) rises with an increase in the content of GO. The increasing in T<sub>m</sub> seems to be related to the lamella nature of GO nanosheets. The increase of GO content in PVP/amylose/GO nanocomposite modified the thermal stability of the films by raising the crystallinity of nanocomposite matrix. By adding GO to the nanocomposite, the melting calorimetric peaks are rather symmetrical than PVP/amylose composite and at the highest load of GO this state is more considerable. This may relate to the main crystallinity shape of GO nanosheets. The results are in close agreement with earlier published results [37].

### 3.2. Weight loss and water uptake of the PVP/amylose/GO

The water absorption capacity of amylose is very considerable because of the hydroxyl groups that located on its macromolecules. The water uptake of PVP/amylose/GO nanocomposites at three different RHs (33, 53 and 81%) was tested and the results are given in Fig. 3. Regardless of the amount of RH, the water uptake ability of the PVP/amylose/GO films decreases when the GO nanosheets content increases due to the GO excellent water-barrier ability. By adding GO, the amylose–amylose macromolecule interactions may decrease. This was consistent with the results of Y. He et al. [6]. In all RH conditions, the addition of GO caused to decrease of the water solubility of the nanocomposite films. Therefore, the water uptake of the PVP/amylose/GO films is lower than that of the PVP/amylose films. This was consistent with the results of Taghizadeh et al. [38].

The GO nanosheets act as a physical barrier against the diffusion of the water molecules to the nanocomposite matrix and causes a meandrous pathway and diminish the length of the free passage for water absorption. This may be due to the GO ability to form hydrogen bonds with amylose and these strong interactions reduce the diffusion of water molecules in the composite. For each RH, by ascending the load of GO, the composite films had the lowest moisture absorbability. These results suggest that the addition of GO improves the water resistance of the PVP/amylose composites. The weight loss of PVP/amylose/GO films in the presence of two different amounts of α-amylase (1 and 3 mg) and at two temperatures (25 and 37 °C) shown in Fig. 4. As seen by increasing the GO content, the amount of weight loss is increased (in accordance with water uptake properties).

On the other hand, Fig. 5 shows the extent of glucose over a 60 h hydrolysis time for each substrate. The rate of glucose production was calculated according to Table 1 by assuming a linear relationship between the concentration of glucose and time for the first 7 h of hydrolysis. Apparently, the GO has a stabilizing effect against the enzymatic attack.

### 3.3. FT-IR spectroscopy

The FTIR spectra for PVP/amylose/GO films are shown in Fig. 6. The chemical modifications, which occur during the enzymatic degradation process, can be evaluated by comparing the FTIR spectra of different conditions. Fig. 6 represents the spectra of the final products of the PVP/amylose/GO nanocomposites in the presence of different GO contents. The samples were immersed in enzymatic solutions for a period of 60 h and then the dried samples prepared for FTIR spectroscopy analysis. The broad band at the range of 3233–3410 cm<sup>-1</sup> is related to the –OH groups and is a result of overlap at stretching of –OH groups settled on the both of amylose and GO molecules. The bands at 1727 and 1622 cm<sup>-1</sup>, are related to carboxyl and carbonyl groups, respectively. The characteristic peak at 1014 cm<sup>-1</sup> is ascribed to the C–O–C glycosidic bond is reported in the literature to be 1150–1040 cm<sup>-1</sup> [39].

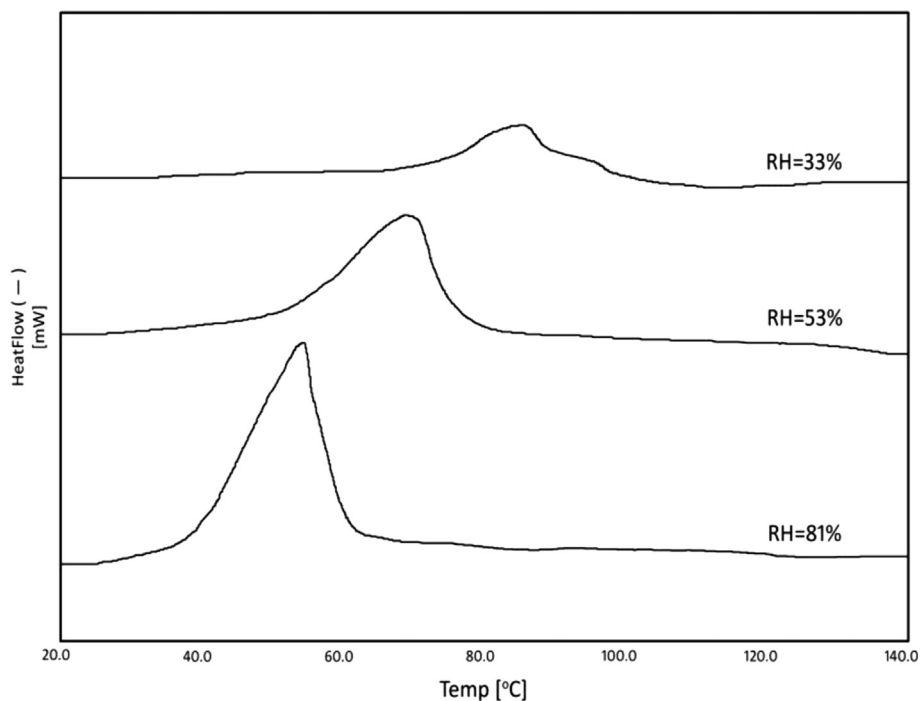


Fig. 1. DSC thermograms for PVP/amylose composites at different relative humidity (RH).

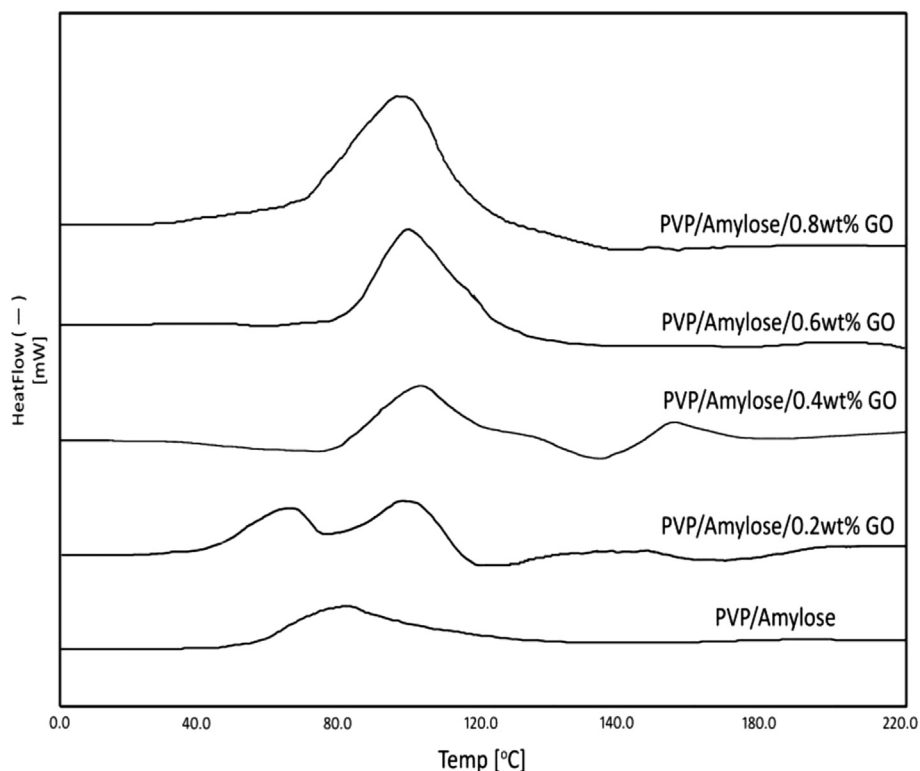


Fig. 2. DSC thermograms for PVP/amylose/GO nanocomposites contained different GO loadings.

The peak at  $713\text{ cm}^{-1}$  is a characteristic band of the C–N stretching associated with the stretch of C–N on the tertiary amide structure of PVP. The peak at  $2923\text{ cm}^{-1}$  is a characteristic band of the C–H stretching associated with the ring methane hydrogen atoms [40]. From Fig. 6 the effect of enzymatic hydrolysis on the

chemical structure of the nanocomposite is considerable. Intensity decline of the band  $1150\text{--}1040\text{ cm}^{-1}$  was observed in the sample immersed in  $\alpha$ -amylase solution, which indicates the cleavage of the  $\alpha$ -(1  $\rightarrow$  4) glycosidic bonds of amylose. However, the increase of GO content that act as a stabilizer, reduce the Amylose–Amylose

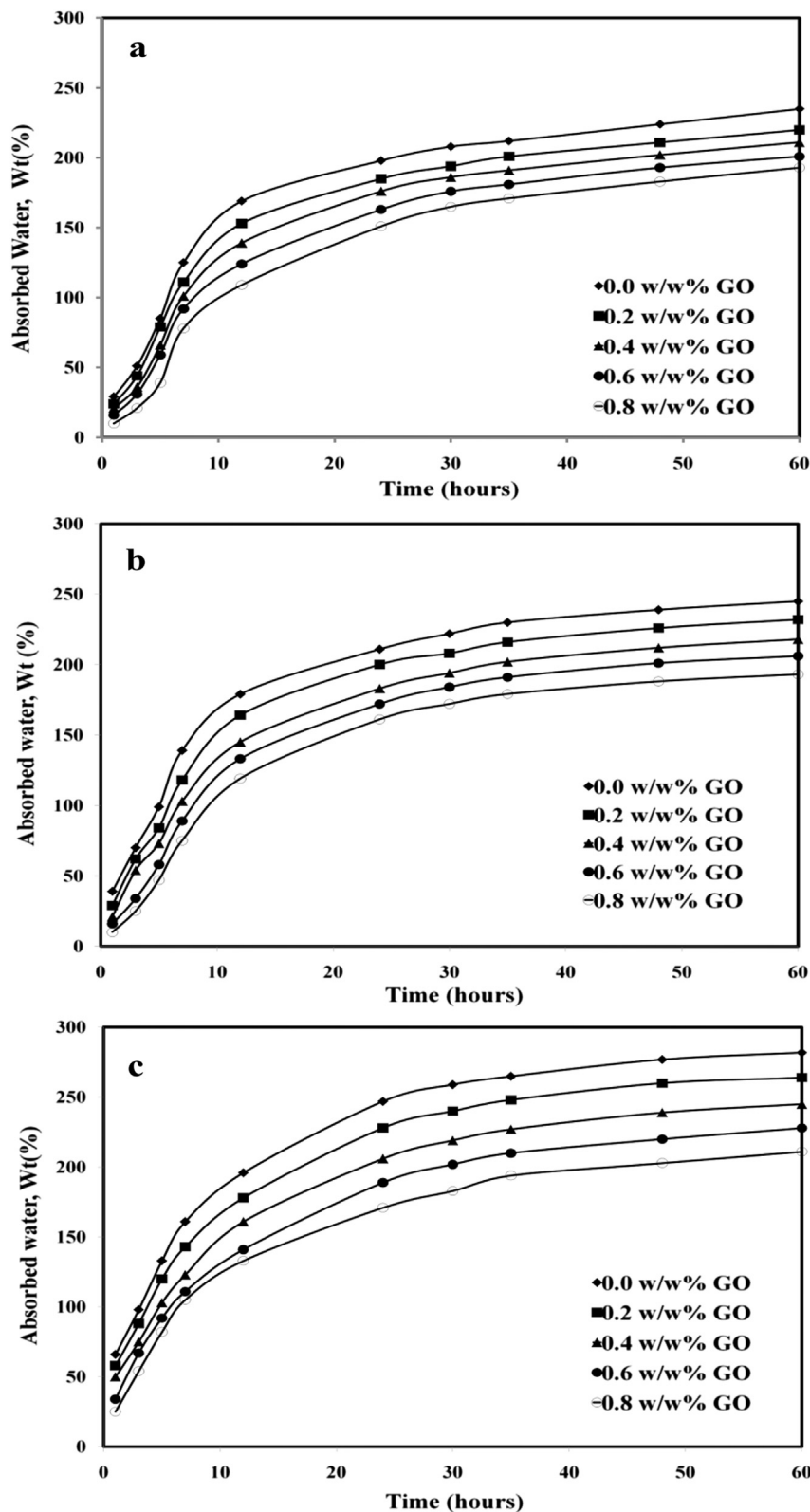


Fig. 3. Water uptake of PVP/amylose/GO nanocomposites with different amounts of GO nanosheets at RH = 33% (a), RH = 53% (b) and RH = 83% (c).

interactions and decrease the hydrolysis of glycosidic bonds, effectively. The increase of intensity on the  $1014\text{ cm}^{-1}$  peak confirmed the stabilization of PVP/amylose on the hydrolysis of the C–O–C bond in the presence of GO nanosheets. Intensity reduction

of C–N band at  $713\text{ cm}^{-1}$  proves that  $\alpha$ -amylase could hydrolysis the C–N bonds. This may be related to the vicinity of C–N bond to the carbonyl group on the tertiary amide ring. The nucleophile nature of C=O group could increase the length of C–N bond and

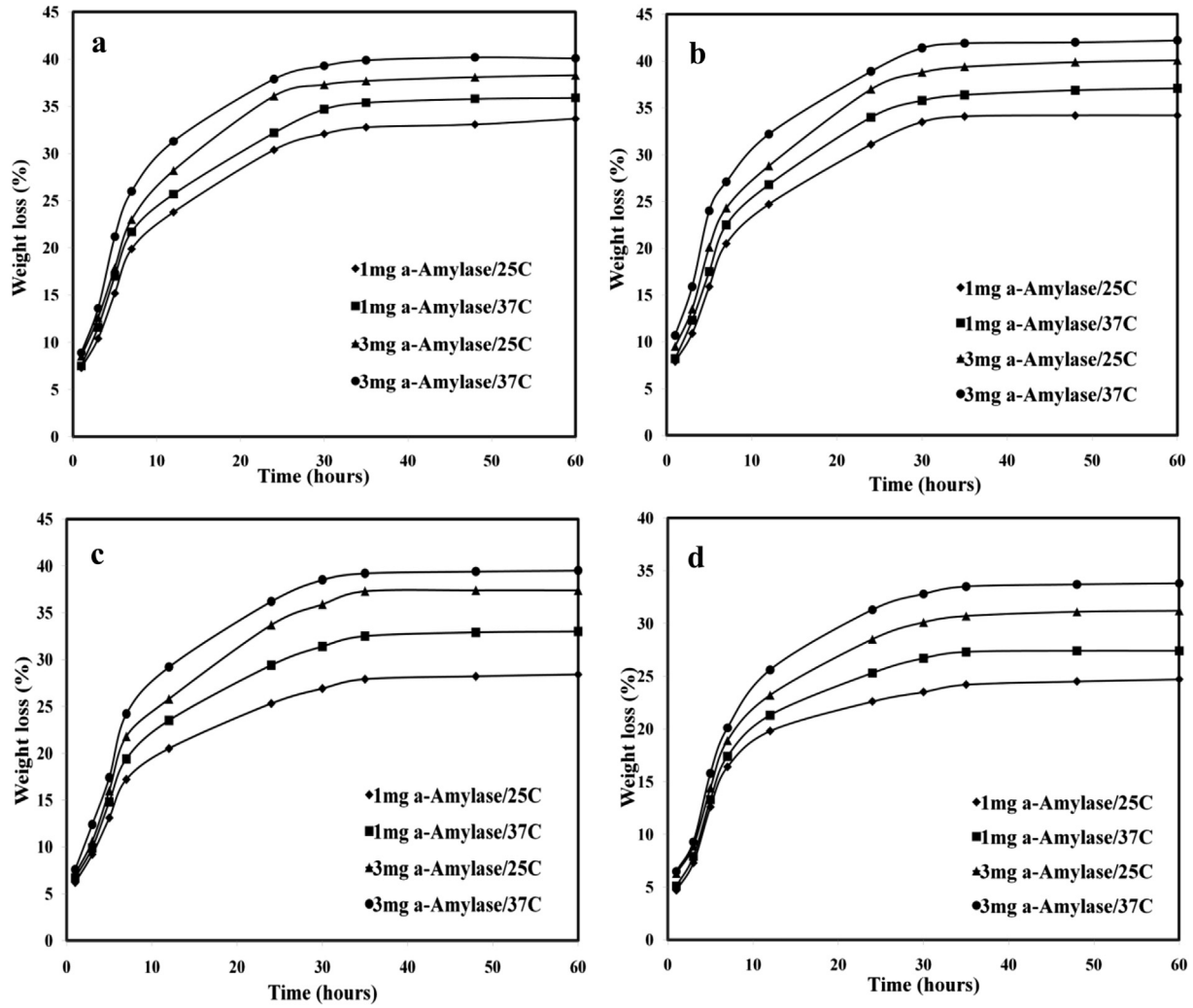


Fig. 4. Weight loss of PVP/amylose/GO nanocomposites in the presence of 1 and 3 mg  $\alpha$ -amyase and at two different temperatures (25 and 37 °C) for (a) 0.2wt%, (b) 0.4wt%, (c) 0.6wt% and (d) 0.8wt% of GO loadings.

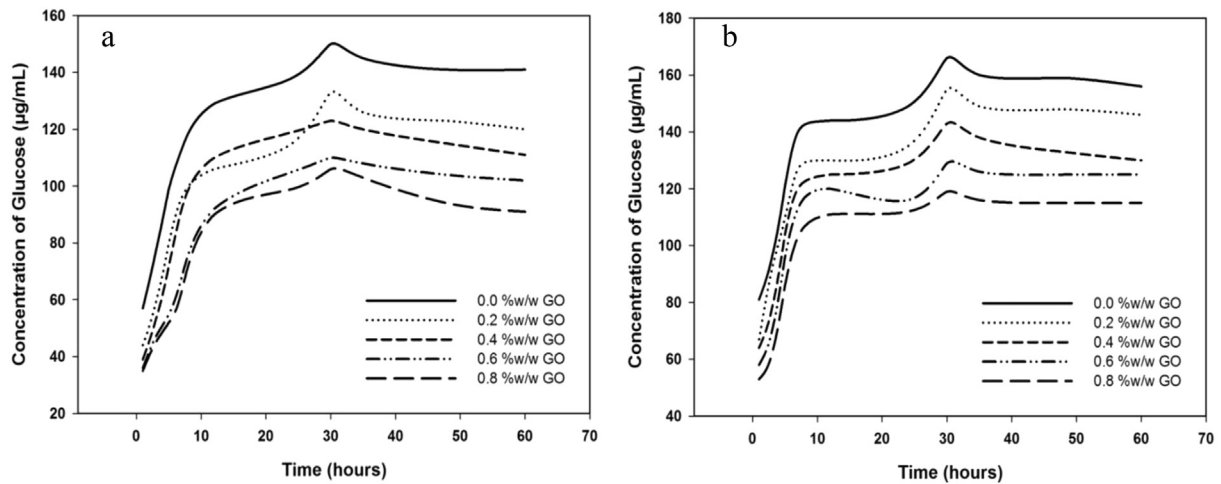


Fig. 5. Concentration of glucose produced for PVP/amylose/GO nanocomposite films in enzymatic degradation due to the action of  $\alpha$ -amyase for different loadings of GO nano-sheets for (a) 1 mg and (b) 3 mg  $\alpha$ -amyase.

**Table 1**

A summary of rates of glucose production due to the action 1 and 3 mg of  $\alpha$ -amylase from each substrates.

Substrate	Rate ( $\mu\text{g/ml h}$ )	
	1 mg $\alpha$ -amylase	3 mg $\alpha$ -amylase
PVP/amylose	9.5	10.1
PVP/amylose/0.2 wt% GO	8.9	9.9
PVP/amylose/0.4 wt% GO	8.8	9.7
PVP/amylose/0.6 wt% GO	5.2	9.5
PVP/amylose/0.8 wt% GO	4.5	8.7

reduce the bond strength. Recently, A.R.C. Duarte et al. investigated on the lipase effect on the hydrolysis of poly-( $\epsilon$ -caprolactone) blended with starch. They found that lipase could result in hydrolysis of C–O bond in the ester group of poly-(3-caprolactone) [41].

### 3.4. X-ray diffraction

Fig. 7 shows X-ray diffractograms for PVP/amylose pure composite films without any additives. This section of investigation is different from other sections because of sonication usage in order to increase the homogeneity of composite matrix. All of the films that used for X-ray analysis formed at RH = 33% and low air humidity. The films formed at low air humidity were almost amorphous, while increased air humidity during film formation resulted in a gradually increased B-type crystallinity [42]. The XRD patterns of the mixture of amylose and PVP after sonication from 10 to 70 W were mainly exhibited B-type XRD pattern while the power of ultrasound was increased. The PVP/amylose blend at the pure state and also the low power of sonication show the V-type crystalline shape (Fig. 7a and b). However, the PVP/amylose composite film sonicated by the power of 70 W exhibited a pure B-type XRD pattern, indicated by the peaks at around 16 and 20°. This might be related to amylose self-recrystallization phenomena that resulted in the high intensity of ultrasonic field. The scission and recombination of

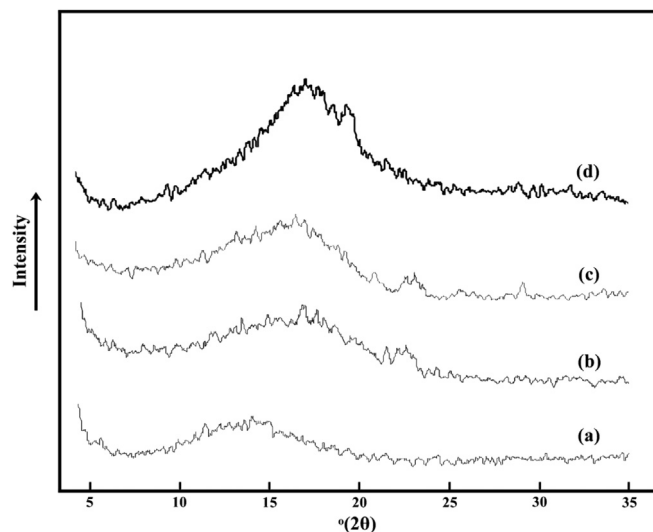


Fig. 7. XRD patterns of pure PVP/amylose without GO nanosheets, treated by different power of ultrasound (a) 10, (b) 30 W, (c) 50 W and (d) 70 W.

polymer chains would take place in the ultrasonic process and this result in a change in crystalline state of polymeric materials [43]. The strain-induced crystallization in the presence of mechanical force could be related to the modification of entropy of activation. As a polymer is stretched, the chains align and the overall entropy of the region decreases. The change in entropy associated with crystallization decreases with respect to the undeformed polymer, thus increasing the rate of crystallization. At the point that crystallization begins, the crystallization rate initially increases as more strain is applied [44].

Fig. 8 shows the XRD patterns for PVP/amylose composite with different GO loadings. As shown in Fig. 6a, the pattern of pure PVP/amylose has a broad peak at 21° and 27° that are related to the main diffractions of this composite. By adding GO to the

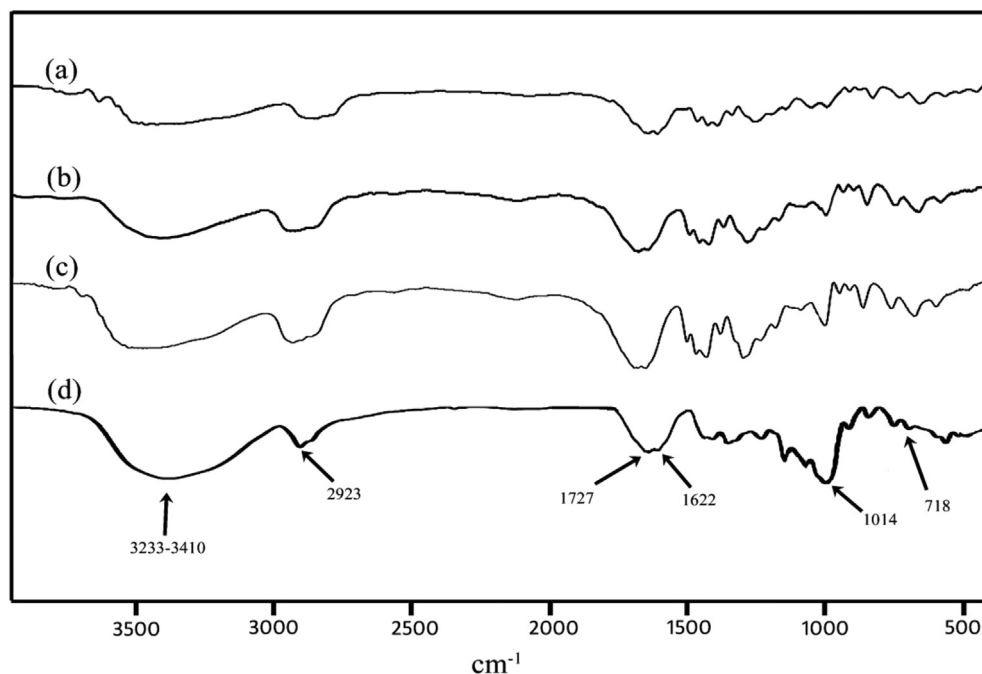
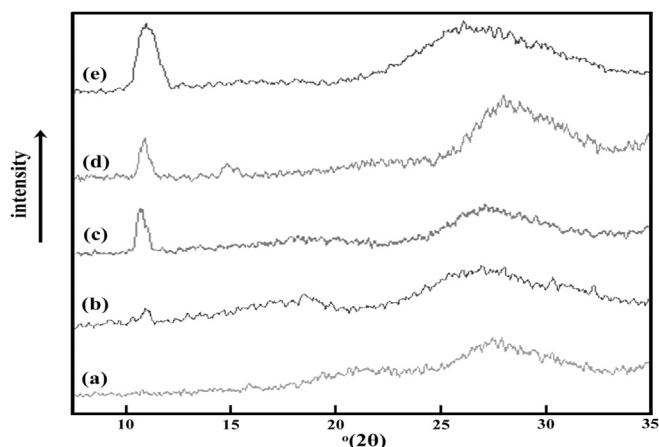


Fig. 6. FTIR spectra of PVP/amylose/GO in the presence of (a) 0.8, (b) 0.6, (c) 0.4 and (d) 0.2 wt% immersed in  $\alpha$ -amylase solution after 24 h.



**Fig. 8.** XRD patterns for pure PVP/amylose composite (a) and for PVP/amylose/GO nanocomposites with different GO loadings, (b) 0.2wt%, (c) 0.4wt%, (d) 0.6wt% and (e) 0.8wt%.

composite matrix, a peak at  $11^\circ$  that presents the retaining of a layered structure in the presence of GO nanosheets (Fig. 6b–d). The intensity of GO peak increased for each 0.2% increase of GO that may be attributed to the adsorption of amylose chain onto the GO nanosheets through hydrogen bonds. This process may lead to the slowing of recrystallization of amylose during the drying process. Furthermore, the XRD patterns show a uniform and exfoliated dispersion of GO nanosheets in the PVP/amylose matrix.

### 3.5. SEM observation of film section

Fig. 9a–f shows a series of representative SEM images obtained after the treatment of the PVP/amylose composite with  $\alpha$ -amylase. The first image (Fig. 9a) was obtained for PVP/amylose before the addition of the enzyme, and is defined as the zero time point. The image reflects the smooth and uniform surface of un-degraded PVP/amylose. After incubation of the PVP/amylose films with the enzyme for 12 min a porous structure is visible in the SEM image (Fig. 9b). The image also reveals that enzymatic degradation result in separation of amylose molecules from the polymer network [45]. Fig. 9c–f were obtained after incubation with the enzyme for 24, 30, 48 and 60 min, and reveals that most of the amylose chains have been degraded, that reveals more porous structure. The images also demonstrate that SEM can be used to follow events altering surface properties, such as enzymatic hydrolysis [46].

## 4. Conclusions

In this study, the effect of GO nanosheets on PVP/amylose composite has been investigated. The water absorption of composite films in the presence of GO was modified and increase as GO content increases and result in more water resistant network of polymer composite. Also, GO act as a good filler and due to its polar groups form hydrogen bonds with amylose that improved the compatibility of PVP/amylose/GO nanocomposite. PVP addition helps to obtain a flexible and stronger polymeric matrix. The FTIR results indicated that  $\alpha$ -amylase activity decreased by increasing the GO content and the scission of glycosidic bond influenced by the amount of GO nanosheets. XRD results indicated that in the case of PVP/amylose composite, crystallinity of the

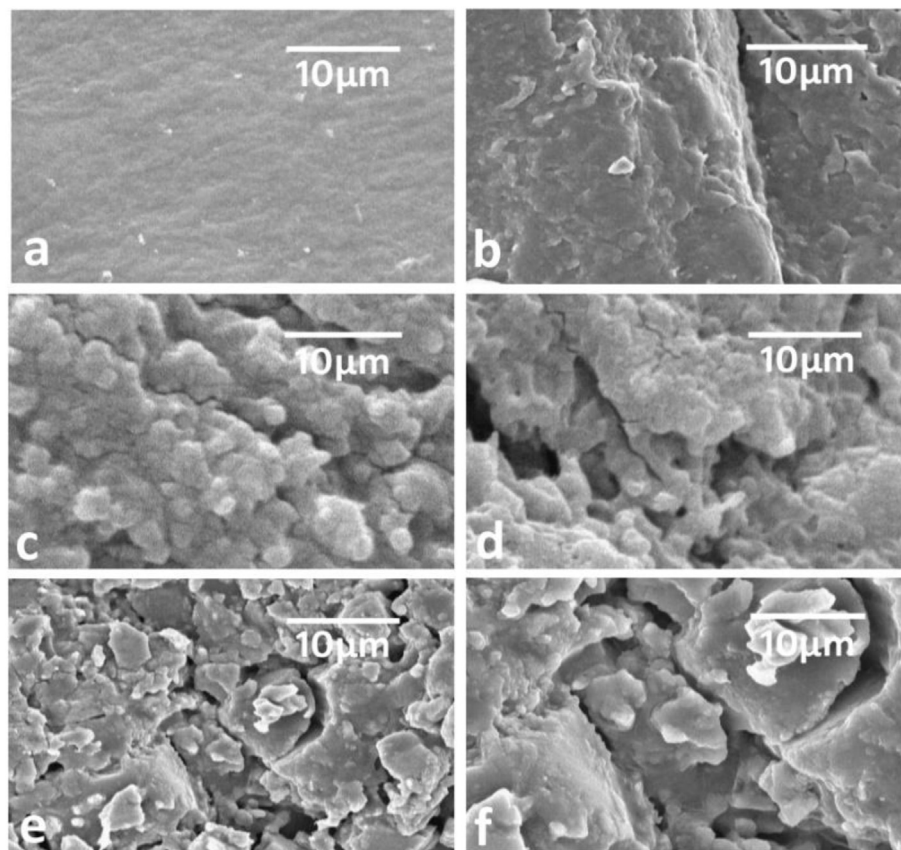


**Fig. 9.** SEM micrographs of PVP/amylose composite in the zero point (a) and hydrolyzed by  $\alpha$ -amylase after (b) 12, (c) 24, (d) 30, (e) 48 and (f) 60 min.

matrix was induced by mechanical effect such as sonication that we used in this study. But in the presence of GO the XRD pattern shows a recrystallization process in the amylose by dispersion of GO nanosheets. The results of DSC show that the peaks move toward lower temperatures as the moisture content of the sample is increased. On the other hand, increase of GO content in PVP/amylose/GO nanocomposite modified the thermal stability of the films via an increase in crystallinity of nanocomposite matrix.

## References

- [1] Spiridon I, Cristina Popescu M, Bodarlaru R, Vasile C. Enzymatic degradation of some nanocomposites of poly(vinyl alcohol) with starch. *Polym Degrad Stab* 2008;93(10):1884–90. <http://dx.doi.org/10.1016/j.polydegradstab.2008.07.017>.
- [2] Fu Z, Wang L, Li D, Wei Q, Adhikari B. Effects of high-pressure homogenization on the properties of starch-plasticizer dispersions and their films. *Carbohydr Polym* 2011;86(1):202–7. <http://dx.doi.org/10.1016/j.carbpol.2011.04.032>.
- [3] Hu G, Chen J, Gao J. Preparation and characteristics of oxidized potato starch films. *Carbohydr Polym* 2009;76(2):291–8. <http://dx.doi.org/10.1016/j.carbpol.2008.10.032>.
- [4] Miles MJ, Morris VJ, Ring SG. Gelation of amylose. *Carbohydr Res* 1985;135(2): 257–69. [http://dx.doi.org/10.1016/S0008-6215\(00\)90777-8](http://dx.doi.org/10.1016/S0008-6215(00)90777-8).
- [5] Jiang S, Li X, Zuo D, Wang H, Liu Z, Xu R. A comparative study on nano  $\text{La}_2\text{O}_3$  suspension treated by ultrasonic and ball milling. *J Rare Earth* 2012;30(11): 1116–22. [http://dx.doi.org/10.1016/S1002-0721\(12\)60190-2](http://dx.doi.org/10.1016/S1002-0721(12)60190-2).
- [6] He Y, Wang X, Wu D, Gong Q, Qiu H, Liu Y, et al. Biodegradable amylose films reinforced by graphene oxide and polyvinyl alcohol. *Mater Chem Phys* 2013;142(1):1–11. <http://dx.doi.org/10.1016/j.matchemphys.2013.05.036>.
- [7] Bittmann B, Hauptert F, Karl Schlarb A. Preparation of  $\text{TiO}_2$ /epoxy nanocomposites by ultrasonic dispersion and their structure property relationship. *Ultrason Sonochem* 2011;18(1):120–6. <http://dx.doi.org/10.1016/j.ultrsonch.2010.03.011>.
- [8] Chen D, Ni S, Chen Z. Synthesis of  $\text{Fe}_3\text{O}_4$  nanoparticles by wet milling iron powder in a planetary ball mill. *China Particuology* 2007;5(5):357–8. <http://dx.doi.org/10.1016/j.cpart.2007.05.005>.
- [9] Prozorov T, Prozorov R, Suslick KS. High velocity interparticle collisions driven by ultrasound. *J Am Chem Soc* 2004;126(43):13890–1. <http://dx.doi.org/10.1021/ja049493o>.
- [10] Mason TJ, Lorimer JP. *Applied sonochemistry*. Weinheim, Germany: Wiley-VCH; 2002.
- [11] Bittmann B, Hauptert F, Schlarb AK. Ultrasonic dispersion of inorganic nanoparticles in epoxy resin. *Ultrason Sonochem* 2009;16(5):622–8. <http://dx.doi.org/10.1016/j.ultrsonch.2009.01.006>.
- [12] Yasmin A, Luo JJ, Daniel IM. Processing of expanded graphite reinforced polymer nanocomposites. *Compos Sci Technol* 2006;66(9):1182–9. <http://dx.doi.org/10.1016/j.compscitech.2005.10.014>.
- [13] Wei CL, Zhang MQ, Rang MZ, Friedrich K. Tensile performance improvement of low nanoparticles filled-polypropylene composites. *Compos Sci Technol* 2002;62(10):1327–40. [http://dx.doi.org/10.1016/S0266-3538\(02\)00079-9](http://dx.doi.org/10.1016/S0266-3538(02)00079-9).
- [14] Geim AK, Novoselov KS. The rise of graphene. *Nat Mater* 2007;6:183–91. <http://dx.doi.org/10.1038/nmat1849>.
- [15] Rao CNR, Sood AK, Subrahmanyam KS, Govindaraj A. Graphene: the new two-dimensional nanomaterial. *Angew Chem Int Ed* 2009;48(42):7752–77. <http://dx.doi.org/10.1002/anie.200901678>.
- [16] Ramanathan T, Abdala AA, Stankovich S, Dikin DA, Herrera-Alonso M, Piner RD, et al. Functionalized graphene sheets for polymer nanocomposites. *Nat Nanotechnol* 2008;3(6):327–31. <http://dx.doi.org/10.1038/nnano.2008.96>.
- [17] Stankovich S, Dikin DA, Dommett GHB, Kohlhaas KM, Zimney EJ, Stach EA, et al. *Nature* 2006;442(7100):282–6. <http://dx.doi.org/10.1038/nature04969>.
- [18] Han D, Yan L, Chen W, Li W. Preparation of chitosan/graphene oxide composite film with enhanced mechanical strength in the wet state. *Carbohydr Polym* 2011;83(2):653–8. <http://dx.doi.org/10.1016/j.carbpol.2010.08.038>.
- [19] Hao R, Qian W, Zhang L, Hou Y. Aqueous dispersions of TCNQ-anion-stabilized graphene sheets. *Chem Commun (Cambridge, U.K.)* 2008;48:6576–8. <http://dx.doi.org/10.1039/b816971c>.
- [20] Li D, Muller MB, Gilje S, Kaner RB, Wallace GG. Processable aqueous dispersions of graphene nanosheets. *Nat Nanotechnol* 2008;3:101–5. <http://dx.doi.org/10.1038/nnano.2007.451>.
- [21] Park S, An J, Piner RD, Jung I, Yang D, Velamakanni A, et al. Aqueous suspension and characterization of chemically modified graphene sheets. *Chem Mater* 2008;20(3):6592–4. <http://dx.doi.org/10.1021/cm801932u>.
- [22] Park S, Ruoff RS. Chemical methods for the production of graphenes. *Nat Nanotechnol* 2009;2:17–24. <http://dx.doi.org/10.1038/nnano.2009.58>.
- [23] Paredes JI, Villar-Rodil S, Martínez-Alonso A, Tascón JMD. Graphene oxide dispersions in organic solvents. *Langmuir* 2008;24(19):10560–4. <http://dx.doi.org/10.1021/la801744a>.
- [24] Fang M, Wang K, Lu H, Yang Y, Nutt S. Covalent polymer functionalization of graphene nanosheets and mechanical properties of composites. *J Mater Chem* 2009;19(38):7098–105. <http://dx.doi.org/10.1039/B908220D>.
- [25] Kong BS, Yoo HW, Jung HT. Electrical conductivity of graphene films with a poly(allylamine hydrochloride) supporting layer. *Langmuir* 2009;25(18): 11008–13. <http://dx.doi.org/10.1021/la901310g>.
- [26] Pan Y, Wu T, Bao H, Li L. Green fabrication of chitosan films reinforced with parallel aligned graphene oxide. *Carbohydr Polym* 2011;83(4):1908–15. <http://dx.doi.org/10.1016/j.carbpol.2010.10.054>.
- [27] Kai WH, Hirota Y, Hua L, Inoue Y. Thermal and mechanical properties of a poly( $\epsilon$ -caprolactone)/graphite oxide composite. *J Appl Polym Sci* 2008;107(3): 1395–400. <http://dx.doi.org/10.1002/app.27210>.
- [28] Xu J, Hu Y, Song L, Wang Q, Fan W, Liao G, et al. Thermal analysis of poly(vinyl alcohol)/graphite oxide intercalated composites. *Polym Degrad Stab* 2001;73(1):29–31. [http://dx.doi.org/10.1016/S0141-3910\(01\)00046-5](http://dx.doi.org/10.1016/S0141-3910(01)00046-5).
- [29] Kim CJ, Khan W, Kim DH, Cho KS, Park SY. Graphene oxide/cellulose composite using NMMO monohydrate. *Carbohydr Polym* 2011;86(2):903–9. <http://dx.doi.org/10.1016/j.carbpol.2011.05.041>.
- [30] Becerril HA, Mao J, Liu Z, Stoltenberg RM, Bao Z, Chen Y. Evaluation of solution-processed reduced graphene oxide films as transparent conductors. *ACS Nano* 2008;2(3):463–70. <http://dx.doi.org/10.1021/nn700375n>.
- [31] Hirata M, Gotou T, Horiuchi S, Fujiwara M, Ohba M. Thin-film particles of graphite oxide 1: high-yield synthesis and flexibility of the particles. *Carbon* 2004;42(14):2929–37. <http://dx.doi.org/10.1016/j.carbon.2004.07.003>.
- [32] Sim B, Zhang WL, Choi HJ. Graphene oxide/poly(2-methylamyl) composite particle suspension and its electro-response. *Mater Chem Phys* 2015;153(1): 443–9. <http://dx.doi.org/10.1016/j.matchemphys.2015.01.039>.
- [33] Rui ZT, Ran L, Xin LL, Ying ZY, Jin LT, Nian YJ. Photochromic polyoxotungstoeuropate K12 [EuP5W3O0110]/Polyvinylpyrrolidone nanocomposite films. *J Solid State Chem* 2003;172(2):458–63. [http://dx.doi.org/10.1016/S0022-4596\(03\)00036-7](http://dx.doi.org/10.1016/S0022-4596(03)00036-7).
- [34] Ramya CS, Selvakarandian S, Hirankumar G, Savitha T, Angelo PC. Investigations on the effect of complexation of naf salt with polymer blend (PEO/PVP) electrolyte ionic conductivity and optical energy band gaps. *J Non-Cryst Solids* 2008;35(4):1494–502. <http://dx.doi.org/10.1016/j.jnoncrysol.2007.08.038>.
- [35] Thiewes HJ, Steeneken PAM. The glass transition and the sub-Tg endotherm of amorphous and native potato starch at low moisture content. *Carbohydr Polym* 1997;32(2):123–30. [http://dx.doi.org/10.1016/S0144-8617\(96\)00133-6](http://dx.doi.org/10.1016/S0144-8617(96)00133-6).
- [36] Pérez A, Sandoval AJ, Cova A, Müller AJ. Glass transitions and physical aging of cassava starch – corn oil blends. *Carbohydr Polym* 2014;105:244–52. <http://dx.doi.org/10.1016/j.carbpol.2014.01.032>.
- [37] Matveev YI, van Soest JG, Nieman C, Wasserman LA, Protserov VA, Ezernitskaja M, et al. The relationship between thermodynamic and structural properties of low and high amylose maize starches. *Carbohydr Polym* 2001;44(2):151–60. [http://dx.doi.org/10.1016/S0144-8617\(00\)0211-3](http://dx.doi.org/10.1016/S0144-8617(00)0211-3).
- [38] Taghizadeh MT, Sabouri N. Study of enzymatic degradation and water absorption of nanocomposites polyvinyl alcohol/starch/carboxymethyl cellulose blends containing sodium montmorillonite clay nanoparticle by cellulase and  $\alpha$ -amylase. *J Taiwan Inst Chem Eng* 2013;44(6):995–1001. <http://dx.doi.org/10.1016/j.jtice.2013.03.012>.
- [39] Pawlak A, Mucha M. Thermogravimetric and FTIR studies of chitosan blends. *Thermochim Acta* 2003;396(1):153–66. [http://dx.doi.org/10.1016/S0040-6031\(03\)00324-1](http://dx.doi.org/10.1016/S0040-6031(03)00324-1).
- [40] *Infrared spectroscopy: fundamentals and applications*, Barbara Stuart. John Wiley & Sons, Ltd; 2004.
- [41] Duarte ARC, Mano JF, Reis RL. Enzymatic degradation of 3D scaffolds of starch-poly-(3-caprolactone) prepared by supercritical fluid technology. *Polym Degrad Stab* 2010;95(10):2110–7. <http://dx.doi.org/10.1016/j.polydegradstab.2010.06.020>.
- [42] Rindlav-Westling A, Stading M, Hermansson AM, Gatenholm P. Structure, mechanical and barrier properties of amylose and amylopectin films. *Carbohydr Polym* 1998;36(2):217–24. [http://dx.doi.org/10.1016/S0144-8617\(98\)00025-3](http://dx.doi.org/10.1016/S0144-8617(98)00025-3).
- [43] Zysman V, Nguyen TQ, Kausch Henning-H. Degradation on freezing dilute polystyrene solutions in p-xylene. *Polym Sci Part B Polym Phys* 1994;32(7): 1257–69. <http://dx.doi.org/10.1002/polb.1994.090320713>.
- [44] Caruso MM, Davis DA, Shen Q, Odom SA, Sottos NR, White SR, et al. Mechanically-induced chemical changes in polymeric materials. *Chem Rev* 2009;109(11):5755–98. <http://dx.doi.org/10.1021/cr9001353>.
- [45] Patrick Gunning A, Giardina TP, Faulds Craig B, Juge Nathalie, Ring Steven G, Williamson Gary, et al. Surfactant-mediated solubilisation of amylose and visualisation by atomic force microscopy. *Carbohydr Polym* 2003;51(2): 177–82. [http://dx.doi.org/10.1016/S0144-8617\(02\)00126-1](http://dx.doi.org/10.1016/S0144-8617(02)00126-1).
- [46] Dimantov Anna, Greenberg Menahem, Kesselman Ellina, Shimoni Eyal. Study of high amylose corn starch as food grade enteric coating in a microcapsule model system. *Innov Food Sci Emerg Technol* 2004;5(1):93–100. <http://dx.doi.org/10.1016/j.ifset.2003.11.003>.